Available online at www.sciencedirect.com
SCIENCE DIRECT®
International Journal of Heat and Mass Transfer 48 (2005) 4161–4173
International Journal of HEAT and MASS TRANSFER
www.elsevier.com/locate/ijhmt

A wall heat transfer model for subcooled boiling flow

Helfried Steiner *, Alexander Kobor, Ludwig Gebhard

Institute of Fluid Mechanics and Heat Transfer, Technical University Graz, Inffeldgasse 25, A-8010 Graz, Austria

Received 18 August 2004; received in revised form 8 February 2005

Abstract

High compactness, low weight and little space requirement are gaining attention as prominent design criteria in the development of modern cooling systems in many applications. The resulting demand for highest possible heat transfer rates has lead to the very promising concept of providing for a controlled transition from pure single-phase convection to subcooled boiling flow in thermally highly loaded regions. For its application in modern engineering design this approach requires a realistic modeling of the complex phenomena associated with the two-phase flow heat transfer. The present work proposes for the computation of the specific wall heat transfer rate a modified superposition model, where the total heat flux is assumed to be additively composed of a forced convective and a nucleate boiling component. Since the present model requires only local input quantities, it is well suited to CFD of geometrically very complex coolant flows, where the definition of global length or velocity scales would be impractical. The wall heat fluxes predicted by the present model were compared against experimental data which were obtained by in-house measurements with water being the working fluid. The overall agreement is very good, particularly, in the partially nucleate boiling regime, where the effect of the bulk flow rate on the heat transfer is significant. Deviations are primarily observed at higher wall superheats, where a strong two-way coupling between the motion of the liquid and the motion of the bubbles as well as considerable bubble–bubble interactions typically occur.

Keywords: Convective flow boiling; Flow-induced suppression; Subcooling

1. Introduction

In the development of modern cooling systems, be it for internal combustion engines, or, for microprocessors, the increasing output of specific power combined with a most compact space- and weight saving design leads to increasingly high thermal loads on the heating surfaces. Thus, wherever a high coolant power with limitations on the available surface area for the heat transfer, the mass flow rate of the liquid coolant as well as the acceptable wall temperatures is to be achieved, a controlled transition to the nucleate boiling regime offers an attractive solution. The concept of exploiting the markedly enhanced heat transfer rates associated with the highly complex phenomenon of evaporation is also a big challenge to the CFD of coolant flows. The computationally very costly concept of direct numerical simulation, which attempts to resolve all physically relevant scales, is applicable only to strongly simplified cases like single bubble configurations (see [1–3]). For engineering

* Corresponding author. Tel.: +43 316 873 7344; fax: +43 316 873 7356.
E-mail address: steiner@fluidmech.tu-graz.ac.at (H. Steiner).

0017-9310/$ - see front matter © 2005 Elsevier Ltd. All rights reserved.
doi:10.1016/j.ijheatmasstransfer.2005.03.032

Nomenclature

b	model constant [–]
c	specific heat [J/kg K]
C_s	constant [–]
d_{hyd}	hydraulic diameter [m]
F	force [N]
g	gravitational acceleration [m/s^2]
G	specific mass flow rate [kg/m^2 s]
G_s	$=(du/dy)(y/u)$ shear rate [–]
h	heat transfer coefficient [W/m^2 K]
h_{lg}	latent heat [J/kg]
k	thermal conductivity [W/m K]
K	constant [–]
m, n	constants [–]
p	pressure [N/m^2]
q	specific heat transfer rate [W/m^2]
r	radius [m]
S	suppression factor [–]
T	temperature [°C]
t	time [s]
u	velocity [m/s]
u_τ	$=\sqrt{\tau_w/\rho}$ wall friction velocity [m/s]
V	volume [m^3]
x	axial coordinate [m]
y	wall normal coordinate [m]
y^+	$=\rho_l u_\tau y/\mu_l$ non-dimensional distance [–]

Greek symbols

α	thermal diffusivity [m^2/s]
κ, χ	constants [–]
μ	dynamic viscosity [kg/m s]
ρ	mass density [kg/m^3]
Φ	correction factor [–]
Ψ	constant [–]
σ	surface tension [kg/s^2]
τ	shear stress [N/m^2]
Θ	angle [rad]
ζ	mass fraction [–]

Subscripts

b	bulk
bcy	buoyancy
d	drag
du	bubble growth
D	departure
fc	forced convection
flow	flow-induced
g	vapour phase
l	liquid phase
L	lift-off
nb	nucleate boiling
onb	onset of boiling
p	constant pressure
s	saturation
sl	shear lift
sub	subcooling
tp	two-phase
trans	transition
w	wall

flow configurations, where the technique of direct numerical simulation has to be ruled out for its high computational cost, computationally feasible and at the same time accurate boiling models have to be provided to obtain reliable numerical results.

The location of subcooled boiling occurring in a channel heated from beneath is sketched for in Fig. 1. The subcooled boiling region extends downstream from a certain location B, where the wall superheat $T_w - T_s$ is sufficient to initiate and sustain nucleate boiling, while the temperature of the bulk liquid T_b remains below the local saturation temperature T_s. The corresponding subcooled boiling segment in the flow boiling curve is schematically shown in Fig. 2. The lower boundary at point B marks the onset temperature T_{onb} of the partially developed boiling (PDB), where the boiling curve starts to deviate from the dashed-dotted extension of the almost straight single-phase line. The heat transfer in the PDB regime is basically dominated by two effects, the macroconvection due to the motion of the bulk liquid and the latent heat transport associated with the

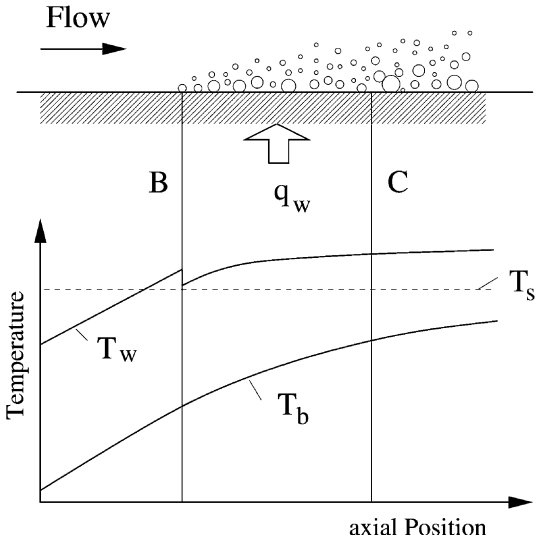

Fig. 1. Subcooled flow boiling domain in a heated channel.

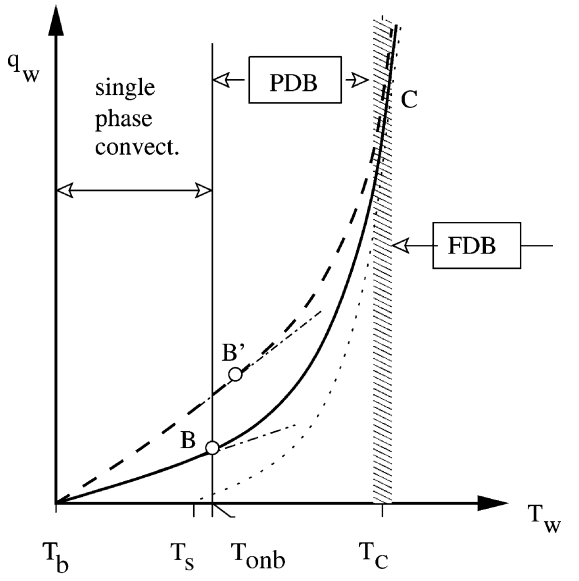

Fig. 2. Flow boiling curves for two bulk velocities: dashed line (– – –) denotes the higher velocity; dotted line (· · ·) denotes the pool boiling curve.

evaporation of the liquid microlayer between the bubble and the heater wall. The important contribution of the macroconvection in the PDB region can be seen from the different paths of the two flow boiling curves representing two different flow rates in comparison to the path of the pool boiling curve, which is associated with zero bulk velocity, being all depicted in Fig. 2. With increasing bulk velocity the onset of nucleate boiling is typically shifted to higher wall superheats, such that the nucleate boiling sets in at point B' instead of B in case of the higher flow rate, as schematically shown in the diagram. At higher wall superheats the influence of the macroconvection becomes less and less pronounced, and the evaporating effect prevails. Accordingly, the flow boiling curves approach the pool boiling curve. The transition to the fully developed boiling (FDB) regime can be localized at a certain position C downstream from the location B as shown in Fig. 1. The corresponding point in the boiling curve diagram shown in Fig. 2 is located at temperature T_C. Beyond this temperature T_C there is a merger of the different flow boiling curves for varying bulk velocity, which indicates that they become practically independent of the actual flow rate.

As already pointed out above the large number and the wide diversity of influences which may essentially affect the nucleate flow boiling practically rule out a strict mathematical description of this phenomenon. Therefore, one has to rely on empirical, or, semi-empirical correlations to capture the basic mechanisms which significantly contribute to the total effective heat transfer. Many models suggested for subcooled flow boiling assume the total wall heat flux q_w to be superimposed of two additive contributions, which can be written as

$$q_w = q_{fc} + q_{nb}. \tag{1}$$

The first term q_{fc} is due to forced convection, the latter q_{nb} is due to nucleate boiling. This concept of additive contributions was first introduced by Rohsenow [4]. In this approach Rohsenow subtracted from the experimentally measured values for the total wall heat flux a convective single phase contribution and attributed the residual term to nucleate boiling. He could further successfully correlate this nucleate boiling component using an equation he had originally proposed for saturated pool boiling. In later approaches due to Bowring [5], Bergles and Rohsenow [6] the subcooled boiling contribution was correlated using a simple power law

$$T_w - T_s = \Psi q_{nb}^m, \tag{2}$$

where Ψ and m are empirical constants to be determined in experiments. Since the system pressure is of major importance for the onset of boiling a prominent class of the power law correlations involves the reduced pressure p_{red} as a key correlation parameter. An early correlation of this type was introduced by Mostinskii [7]. Cooper [8], Leiner and Gorenflo [9] and Leiner [10], proposed formulations, which account for surface roughness, as well.

Rather than assuming the additive composition (1) an alternative group of models suggests a geometrical combination of the basic contributions. Models of this type formulate the effective heat transfer coefficient as some product function which can be generally written as

$$h_{tp} = h_{fc}\Phi_{tp}, \tag{3}$$

where the Φ_{tp} represents a correction function due to nucleate boiling. Correlations of this type as suggested by Kandlikar [11], or, by Shah [12], mostly distinguish between the partially and the fully developed boiling regime. Accordingly, they propose different correlations for each regime, which in turn requires an a priori specification of the point of transition from the PDB to the FDB regime.

Among the superposition models of type (1) the model proposed by Chen [16] is widely used today especially in engineering applications in the automotive industry. Chen's model was originally developed for saturated boiling flow. Later, it was extended by Butterworth [17] to the subcooled regime, where it also produced results with acceptable accuracy. In his approach Chen advanced his predecessors' superposition models by accounting explicitly for the interaction between the liquid and the vapour phase. In particular, he distinguished two competing effects on the outcome of total wall heat flux, the enhanced convective transport due to bubble agitation, and the flow-induced

suppression of the nucleate boiling. To the first effect Chen attributed minor importance in the subcooled boiling regime, and, therefore, it need not be explicitly accounted for. The latter flow-induced suppression effect is modelled by Chen in terms of a suppression factor which reduces the nucleate boiling component especially in the PDB regime. Basically, the introduction of such a suppression factor in order to bridge the region between pure single-phase forced convection and fully developed nucleate boiling has the advantage that it circumvents the determination of the point of transition from PDB to the FDB regime, which mostly relies on a lot of empiricism. On the other hand the suppression factor proposed by Chen depends on the bulk flow Reynolds number as the only correlation parameter, which bears two drawbacks. First, imposing only the bulk flow Reynolds number as correlation parameter the suppression model is practically based on a single-phase bulk flow quantity, which makes it incapable to account for important effects like the influence of the liquid phase flow field on the near-wall motion of the bubbles, or, the influence of the wall superheat. The correlation is therefore expected to be very case dependent. Secondly, in the CFD of complex flow geometries it is hardly possible to define a reasonable bulk flow Reynolds number. The boiling departure lift-off (BDL) model, which is presented in this work, was devised to improve Chen's superposition approach, in that it attempts to model the flow-induced suppression on a physically sounder base. The suggested correlation for the flow-induced suppression depends only on local flow quantities which are in general knowns in the numerical solution of the liquid phase flow field. The impact of the subcooling, which is very pronounced at small flow rates combined with low superheats, is accounted as well through an additional parameter. The predictive capability of the BDL model is evaluated by comparing its predictions with experimental data. These data have been obtained in-house in boiling flow experiments. A detailed description of the experimental apparatus used for these measurements is given in Section 2. The description of the mathematical formulation for the BDL model is presented in Section 3.

2. Experimental setup

The present experimental apparatus was designed to investigate subcooled convective boiling at conditions, which are typically met in liquid coolant systems of internal combustion engines. The forced convective flow loop is schematically shown in Fig. 3. The flow is generated by a pump feeding a tank, where the working fluid is preheated to sustain a certain bulk temperature in the test section. The operating pressure is set to a fixed level using a pressure control vessel. The velocity of the bulk

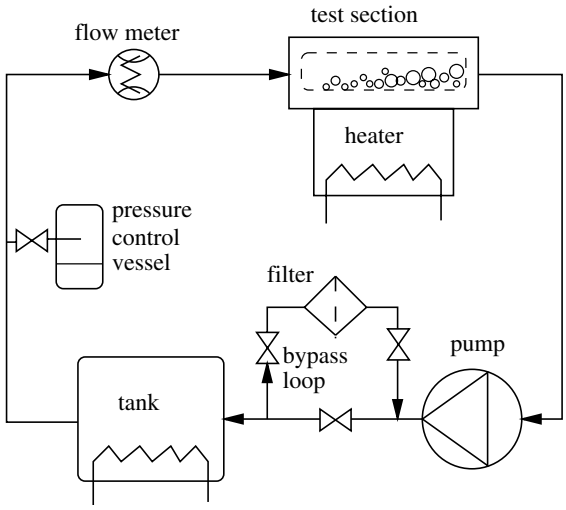

Fig. 3. Schematic diagram of the entire convective boiling flow loop.

flow is controlled by means of an inductive flow meter, whose output is used to adjust the volumetric flow rate via the speed of the feeding pump and/or the flow-rate through the by-pass loop. The present configuration allows the bulk velocity to be varied within the range of $0.05 \leqslant u_b \leqslant 2.0$ m/s. The absolute operating pressure can be set within the range $1.0 \leqslant p \leqslant 2.0$ bar. Small bubbles as well as particle contaminations are sieved out by a filter.

Fig. 4 gives a schematic view inside the test section of the channel. The test section is a square duct with a

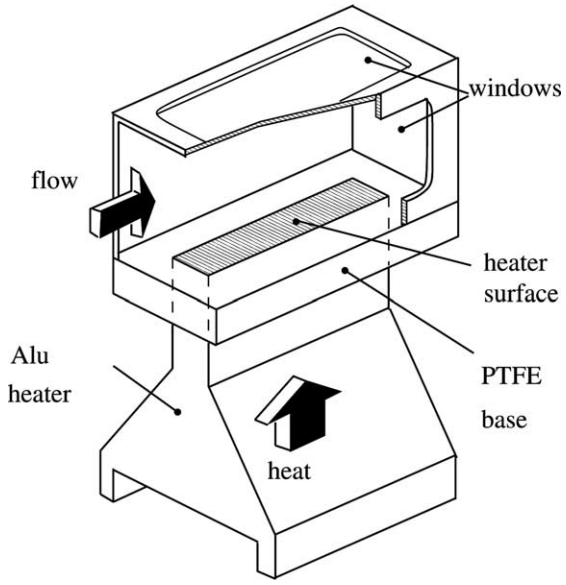

Fig. 4. Test section of the experimental facility.

height of 40 mm and a width of 30 mm. The heat flux into the channel is generated by heating coils located at the bottom of the aluminium heater from where it is conducted to the top of the heater. At the upper surface, whose length is 60 mm and width is 10 mm, respectively, the heat is transferred to the working fluid flowing through the channel. The wall temperature as well as the wall heat flux are determined based on measurements of the temperature using several K-type thermocouples appropriately distributed in the solid heater. The base plate of the test section, where the top of the aluminium heater is built in, is made of PTFE. The outstandingly low thermal conductivity ($\lambda_{\mathrm{PTFE}} = 0.23$ W/m K) of this material should guarantee the lowest possible heat loss of the heater to the surrounding structure. Due to thermal durability restrictions of the PTFE base plate the maximum heater surface temperature was limited to $T_{\mathrm{w}} = 160\,^{\circ}\mathrm{C}$. Below this temperature the observed thermal deformations of the PTFE-structure always remained within an acceptable range. Windows made of glass are embedded in the top as well as the side walls of the test channel to make the heater surface optically accessible. Using the present configuration the total error in the experimentally obtained heat fluxes are mainly due to measurement and position errors of the thermocouples, as well as the uncertainties in the actual thermal conductivity of the heater material (aluminium alloy) and in the heat losses to the surroundings of the heater. A worst-case estimation turned out a total error for the heat flux ranging from ±5% in the convective regime to ±2% in the nucleate boiling regime always referring the value actually obtained from the measurements. The error in the measured surface temperatures amounts to ±0.15 °C. The inductive flow meter measures the flow rate with high accuracy, such that the relative error is only ±0.5% of the displayed value.

3. Mathematical formulation of the subcooled boiling flow model

The BDL model invokes an additive ansatz as suggested by Chen [16] for the total wall heat flux

$$q_{\mathrm{w}} = q_{\mathrm{fc}}\Phi + q_{\mathrm{nb}}S, \tag{4}$$

where the two correction parameters Φ and S modify the forced convection heat flux q_{fc} and the nucleate boiling heat flux q_{nb}, respectively. Both heat fluxes are computed following Chen's proposal. Accordingly, the first is written as

$$q_{\mathrm{fc}} = h_{\mathrm{fc}}(T_{\mathrm{w}} - T_{\mathrm{b}}), \tag{5}$$

where the transfer coefficient h_{fc} is calculated using the Dittus–Boelter equation

$$Nu_{\mathrm{fc}} = \frac{h_{\mathrm{fc}} d_{\mathrm{hyd}}}{\lambda_{\mathrm{l}}} = 0.023 Re_{\mathrm{l}}^{0.8} Pr_{\mathrm{l}}^{0.4} \tag{6}$$

involving the bulk flow Reynolds number and the Prandtl number of the liquid phase

$$Re_{\mathrm{l}} = \frac{\rho_{\mathrm{l}} u_{\mathrm{b}} d_{\mathrm{hyd}}}{\mu_{\mathrm{l}}}, \quad Pr_{\mathrm{l}} = \frac{\mu_{\mathrm{l}} c_{p,\mathrm{l}}}{\lambda_{\mathrm{l}}},$$

respectively. The nucleate boiling heat flux

$$q_{\mathrm{nb}} = h_{\mathrm{nb}}(T_{\mathrm{w}} - T_{\mathrm{s}}) \tag{7}$$

is obtained using a correlation due to Forster and Zuber [18]

$$h_{\mathrm{nb}} = 0.00122 \frac{\lambda_{\mathrm{l}}^{0.79} c_{p,\mathrm{l}}^{0.45} \rho_{\mathrm{l}}^{0.49}}{\sigma^{0.5} \mu_{\mathrm{l}}^{0.29} h_{\mathrm{lg}}^{0.24} \rho_{\mathrm{g}}^{0.24}} \Delta T_{\mathrm{s}}^{0.25} \Delta p_{\mathrm{s}}^{0.75}, \tag{8}$$

where the saturation pressure difference corresponding to the superheat temperature is written as

$$\Delta p_{\mathrm{s}} = p_{\mathrm{s}}(T_{\mathrm{w}}) - p_{\mathrm{s}}(T_{\mathrm{s}}).$$

The factor Φ occurring in Eq. (4) represents the enhancement of the convective component due to bubble agitation. Chen [16] derived a graphic relationship for Φ as a dependent of the inverse of the Martinelli number X_{tt}, which reads

$$\left(\frac{1}{X_{tt}}\right) = \left(\frac{\zeta_{\mathrm{g}}}{1-\zeta_{\mathrm{g}}}\right)^{0.9} \left(\frac{\rho_{\mathrm{l}}}{\rho_{\mathrm{g}}}\right)^{0.5} \left(\frac{\mu_{\mathrm{g}}}{\mu_{\mathrm{l}}}\right)^{0.1}, \tag{9}$$

where ζ_{g} denotes mass fraction of the vapour. Butterworth [17] fitted this relationship $\Phi = \Phi(1/X_{tt})$ with

$$\begin{aligned} &\zeta_{\mathrm{g}} > 0.1 : \Phi = 2.35\left(\frac{1}{X_{tt}} + 0.213\right)^{0.736} \\ &\zeta_{\mathrm{g}} \leqslant 0.1 : \Phi = 1. \end{aligned} \tag{10}$$

In subcooled boiling flow the vapour mass fractions are typically small, such that $\zeta_{\mathrm{g}} \leqslant 0.1$ applies and Φ can be assumed unity.

The essential difference between Chen's approach and the present BDL concept consists in the modeling of the modification of the nucleate boiling component in terms of the factor S in Eq. (4). Chen introduced this parameter S as a flow-induced suppression factor, which he correlated as an empirical function of the product $Re_{\mathrm{l}}\Phi^{1.25}$. This correlation was later fitted by Butterworth [17] with the expression

$$S_{\mathrm{Chen}} = \frac{1}{1 + 2.53 \times 10^{-6} (Re_{\mathrm{l}}\Phi^{1.25})^{1.17}}. \tag{11}$$

For subcooled boiling flow, where $\Phi \approx 1$, the factor S_{Chen} obviously depends on the bulk flow Reynolds number only. In contrast to Chen's bulk-flow dependent, hence, basically global, approach the BDL model attempts to model the flow-induced suppression based on the local dynamics of a vapour bubble subject to the surrounding flow field near the heater surface. Thereby, the BDL model utilizes a concept which was originally proposed by Zeng et al. [19] to compute the

size of a bubble at the point of detachment from the heater surface. According to the hypothesis of Zeng and his coworkers the whole process of vapor bubble detachment basically evolves in three different stages, as schematically shown in Fig. 5. At the first stage the bubble is attached to its nucleation site, and it is inclined by the angle Θ due to the hydrodynamic flow forces. The attached bubble is growing until it reaches a critical departure volume V_D, where the bubble is dragged off its nucleation site. At the point of departure the volume equivalent departure radius is defined as

$$r_D = \left(\frac{3V_D}{4\pi}\right)^{\frac{1}{3}}.$$

The departure from the nucleation site marks the beginning of the stage II, where the departed bubble slides in upright posture ($\Theta = 0$) along the heater surface. Thereby, the bubble still keeps growing in size until it reaches a bubble volume, where the buoyancy force is sufficiently high to make the bubble lift-off from the surface. At the point of the bubble's lift-off the stage III begins and the corresponding lift-off volume V_L determines the volume equivalent lift-off radius defined as

$$r_L = \left(\frac{3V_L}{4\pi}\right)^{\frac{1}{3}}.$$

The departure radius r_D as well as the inclination angle Θ are mathematically obtained by solving the momentum balance equations right at the instant of departure, which are written in the x- and y-direction as

$$0 = F_d + F_{du}\sin\Theta, \tag{12}$$

$$0 = F_{bcy} + F_{du}\cos\Theta + F_{sl}, \tag{13}$$

respectively. Therein, ought to the small density ratio $\frac{\rho_g}{\rho_l} \ll 1$ the inertial forces were neglected, such that the Eqs. (12) and (13) basically represent a static force balance. All the forces which are assumed to be relevant at the point of departure, and, therefore, have to be accounted for are schematically shown in Fig. 6. The considered forces are the drag force F_d, the shear-lift force F_{sl}, the buoyancy force F_{bcy}, and the bubble growth force F_{du}. The surface tension force was assumed to be negligibly small at the moment of departure and omitted. The drag force and the shear-lift force are given by

$$F_d = 6\pi\mu_l u r\left\{\frac{2}{3} + \left[\left(\frac{12}{Re_b}\right)^n + 0.796^n\right]^{-\frac{1}{n}}\right\}, \quad \text{with } n = 0.65 \tag{14}$$

and

$$F_{sl} = \frac{3.877}{2}\rho_l u^2 \pi r^2 G_s^{\frac{1}{2}}\left(\frac{1}{Re_b^2} + 0.014G_s^2\right)^{\frac{1}{4}}, \tag{15}$$

where

$$Re_b = \frac{\rho_l u 2r}{\mu_l} \quad \text{and} \quad G_s = \left|\frac{du}{dy}\right|_{y=r}\frac{r}{u}$$

denote the bubble Reynolds number and the shear rate, respectively. As for the velocity u as well as its spatial derivative $\frac{du}{dy}$, whose values at the location $y = r$ are needed in Eqs. (14) and (15), the presence of the vapour bubbles is neglected such that Reichardt's analytical expression for single-phase flow

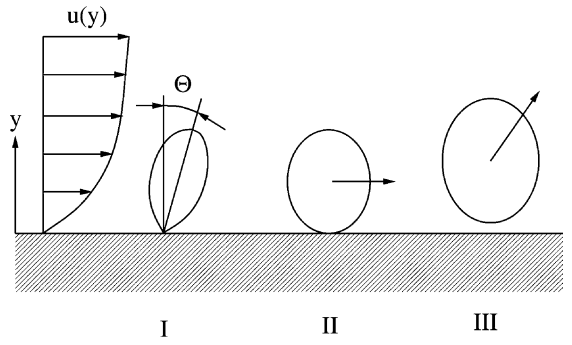

Fig. 5. Three stages of a vapor bubble departing from the heater surface: (I) instant of departure from the nucleation site, (II) sliding bubble, (III) instant of lift-off.

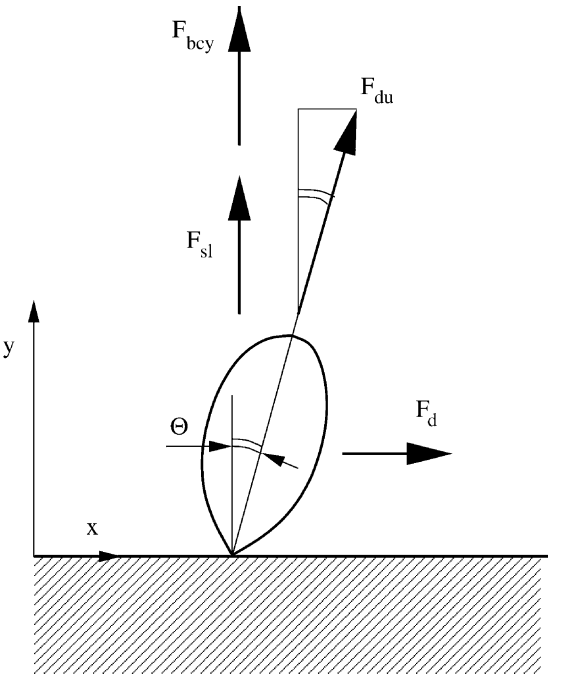

Fig. 6. Force balance at a vapor bubble at the instant of departure from its nucleation site.

$$u^+ = \frac{u}{u_\tau} = \frac{1}{\kappa}\ln(1+\kappa y^+) + C\left[1-\exp\left(-\frac{y^+}{\chi}\right)-\frac{y^+}{\chi}\exp\left(-\frac{y^+}{3}\right)\right] \quad (16)$$

can be used to provide the velocity profile of the liquid phase. Eq. (16) is written as a non-dimensional function of the wall coordinate

$$y^+ = \frac{\rho_l u_\tau y}{\mu_l}$$

with the wall friction velocity

$$u_\tau = \left(\frac{\tau_w}{\rho_l}\right)^{\frac{1}{2}}$$

being determined by the wall shear stress τ_w. The constants are set to $\kappa = 0.41$, $\chi = 11$, and $C = 7.4$, respectively.

The buoyancy force is given by

$$F_{bcy} = \frac{4}{3}r^3\pi g(\rho_l - \rho_g). \quad (17)$$

The bubble growth force F_{du} is modeled following Zeng et al. [21], who considered a hemispherical bubble expanding in an inviscid liquid. They proposed the equation

$$F_{du} = -\rho_l \pi r^2\left(\frac{3}{2}C_s\dot{r}^2 + r\ddot{r}\right), \quad (18)$$

where the empirical constant C_s was introduced to account primarily for the presence of the wall. Based on a comparison with experimental data available to them the authors suggested to set $C_s = \frac{20}{3}$. The temporal evolution of the bubble radius $r(t)$, as well as its temporal derivatives $\dot{r}$ and $\ddot{r}$ needed in Eq. (18), are obtained assuming a diffusion controlled bubble growth model due to Zuber [20], which reads

$$r(t) = \frac{2b}{\sqrt{\pi}}Ja\sqrt{\alpha_l t}, \quad (19)$$

involving the Jakob number

$$Ja = \frac{\rho_l c_{p,l}(T_w - T_s)}{\rho_g h_{lg}},$$

the thermal diffusivity of the liquid phase α_l, and the empirical constant b.

The lift-off radius of the bubble r_L is obtained by solving the momentum balance equations (12) and (13) under the assumption that at the instant of lift-off there is no slip in the velocity between the bubble and the surrounding liquid phase. This implies a zero drag and shear-lift force, and a zero inclination angle, $\Theta = 0$, $F_d = 0$, $F_{sl} = 0$, respectively, such that r_L is obtained upon the solution of

$$0 = F_{bcy} + F_{du}. \quad (20)$$

The predicted bubble radii were compared to experimental data measured at a given wall superheat $\Delta T_s = 29\,^\circ\mathrm{C}$ for four different velocities $u_b = 0.05$, 0.39, 0.77, 1.17 m/s, respectively. Thereby, the growth rate parameter occurring in Eq. (19) was set to $b = 0.21$. The wall friction velocities u_τ needed as input by the model in Eq. (16) were obtained from LDA measurements of the axial velocity component in the plane of symmetry of the test channel right before the beginning of the heater surface. The bubble radii were measured optically using video records. The results of these bubble size measurements are depicted as vertical bars in Fig. 7. Bubble size data taken from a recent very detailed experimental investigation on the bubble dynamics in subcooled boiling flow made by Maurus [22] are shown as well. Maurus measured the bubble radii distribution functions near the wall at a subcooling of $\Delta T_{sub} = 20\,^\circ\mathrm{C}$, which is comparable to the subcooling of the present in-house measurements being $\Delta T_{sub} = 16\,^\circ\mathrm{C}$. It is important to note that the open symbols in Fig. 7 represent the median bubble radii from Maurus' measurements with varying bulk flow rate and a constant wall heat flux of $q_w = 0.77\ \mathrm{MW/m^2}$. This heat flux is considerably higher than in the present experiments, where the bubble size data were obtained at a heat flux in the range of $q_w = 0.40$–$0.45\ \mathrm{MW/m^2}$. The higher heat flux evidently leads to larger bubble radii in Maurus' data as well as to a slower decrease in bubble size with increasing velocity. The here manifested dependence of the mean bubble size on heat flux is also confirmed by

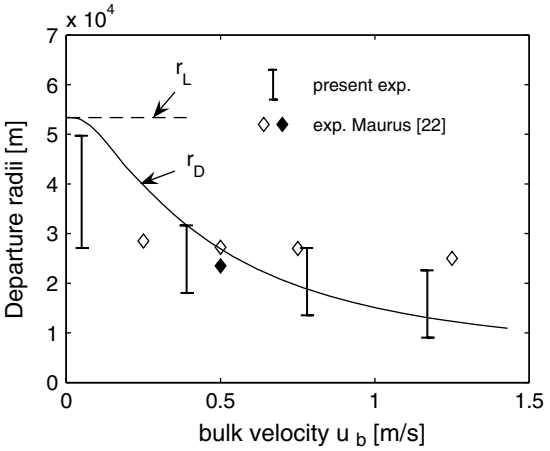

Fig. 7. Full line, '—', predicted departure radii r_D; dashed line, '– –', predicted lift-off radius r_L; bars, 'I', denote the range of the departure radii at a given bulk velocity u_b measured in the present experiments; symbols denote the median bubble radii experimentally obtained by Maurus [22] at a given wall heat flux q_w: open diamonds, '◇' $q_w = 0.77\ \mathrm{MW/m^2}$; filled diamond, '◆', $q_w = 0.37\ \mathrm{MW/m^2}$.

a further set of Maurus' measurements, where the heat flux was varied and the specific mass flow rate was kept constant at $G = 500\ \mathrm{kg/m^2\,s}$. Referring to these measurements the filled symbol represents the median bubble radius obtained for $q_w = 0.37\ \mathrm{MW/m^2}$ which is very close to the range in our own present experiments. It becomes evident that due to the lower heat flux the bubble median radius lies notably below the corresponding value obtained for $q_w = 0.77\ \mathrm{MW/m^2}$ (represented by the open symbol above). Ought to the comparable magnitude of the imposed heat flux the agreement with the present in-house measurements is better for this case as well.

The comparison of the model predictions for the departure radii with the corresponding experimental data exhibits a good agreement for the higher velocities, while deviations occur at the lowest velocity considered. Both modelled radii become equal, i.e., $r_D = r_L$, in the limit of zero bulk velocity. With increasing flow rate the departure radius r_D decreases markedly relative to the lift-off radius r_L. The widening gap between these two radii with increasing bulk velocity evidently reflects the influence of the local velocity field on the bubble detachment process from the surface. Based on this consideration the BDL model correlates the flow-induced suppression in terms of the ratio $\frac{r_D}{r_L}$, and the corresponding suppression factor is proposed as

$$S_{\mathrm{flow}} = \frac{r_D}{r_L}. \tag{21}$$

According to its definition S_{flow} is supposed to represent the flow-induced deviation of the bubble departure radius from the corresponding pool boiling limit, which is associated with zero bulk velocity, where $r_D = r_L$ and, hence, $S_{\mathrm{flow}} = 1$. The present formulation for the computation of r_D and r_L does not explicitly account for subcooling. Thus, the obtained radius r_L basically represents the lift-off radius in the saturated boiling regime and not in the subcooled boiling regime as it is considered in the present configuration. This also explains the overprediction for the bubble sizes in the very low velocity range shown in Fig. 7. It is reasonable to assume that even at very small flow rates the advection of subcooled bulk liquid is sufficient to maintain a subcooled thermal boundary layer, where the departing bubbles are typically smaller than in the saturated case. Accordingly, the experimentally measured departure radii tend towards a limit markedly below the predicted lift-off radius r_L representing the saturated case.

The BDL model accounts for the effect of subcooling by introducing the factor

$$S_{\mathrm{sub}} = \frac{T_w - T_s}{T_w - T_b}. \tag{22}$$

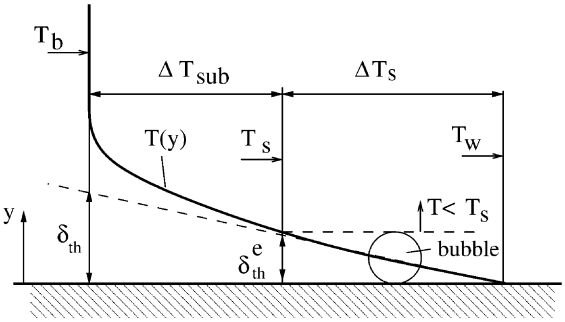

Fig. 8. Superheated thermal boundary layer in subcooled boiling.

The present definition of (22) is based on the concept of a so-called "extrapolated superheat layer thickness" suggested by Wiebe and Judd [23]. As it can be seen in the sketch of the superheated boundary layer in Fig. 8, the extrapolated superheat layer thickness, δ_{th}, is defined as the height of intersection between the tangent to the temperature profile at the wall and the bulk temperature T_b. It is written as

$$\delta_{\mathrm{th}} = \frac{T_w - T_b}{\left.\frac{dT}{dy}\right|_w} \tag{23}$$

and is supposed to reflect closely the superheated layer, which strongly governs the whole process of bubble nucleation, growth and departure. It further becomes evident from Fig. 8 that due to the subcooling a considerable portion of δ_{th} exhibits a temperature lower than the saturation temperature T_s. The growing vapor bubbles cannot protrude into this subcooled layer, because condensation sets in at the bubble tip, once it reaches the zone, where $T < T_s$. Considering this limitation on the bubble size due to the subcooling an "*effective* extrapolated superheat layer thickness"

$$\delta^e_{\mathrm{th}} = \frac{T_w - T_s}{\left.\frac{dT}{dy}\right|_w} \tag{24}$$

can be defined replacing in (23) the bulk temperature T_b by the saturation temperature T_s. The factor S_{sub} given by (22) is then obtained as the ratio $\delta^e_{\mathrm{th}}/\delta_{\mathrm{th}}$ representing thus a measure for the subcooling. The factor S_{sub} is at maximum unity in the case of saturated boiling, where $T_b = T_s$, and it decreases to zero for increasing subcooling $\Delta T_{\mathrm{sub}} = T_s - T_b$.

It is noted that in the choice of the empirical parameter b occurring in (19) the value $b = 0.21$ yielded the best fit to the experimentally measured bubble radii. Basically, this model constant is supposed to account for the asphericity of the bubbles and is of the order of unity. Zeng et al. [19] considered flow boiling data for the refrigerant R113 and obtained the best overall

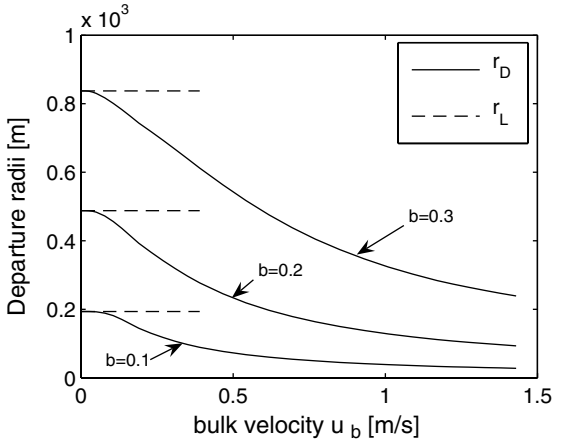

Fig. 9. Predicted departure and lift-off radii for a varying model parameter b.

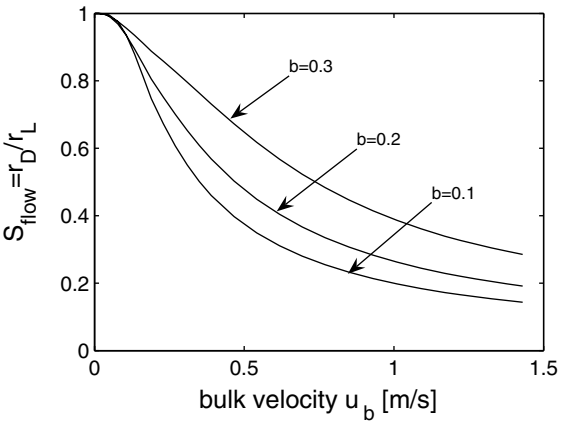

Fig. 10. Flow-induced suppression factor S_{flow} obtained for a varying model parameter b.

agreement with $b = 1$. The sensitivity of the predictions for the bubble size to a variation of b and its effect on the resulting suppression factor S_{flow} is illustrated in Figs. 9 and 10, respectively. It becomes evident that the model parameter b essentially determines the level of the predicted bubble lift-off radius. The suppression factor S_{flow} represents by definition the flow-induced decrease of the departure radius relatively to the corresponding lift-off radius. Depending thus on the ratio of the predicted radii and not explicitly on the predicted individual numerical values, the factor S_{flow} is to some extent less sensitive to the choice of b. As it can be seen from Fig. 10, there is, however, still the tendency that smaller values for b basically produce a smaller flow-induced suppression factor S_{flow}.

Substituting the two suppression factors defined in Eqs. (21) and (22) as total suppression into Eq. (4) the total wall heat flux is then rewritten as

$$q_{\text{w}} = q_{\text{fc}} + q_{\text{nb}} S_{\text{flow}} S_{\text{sub}}. \tag{25}$$

4. Comparison of the model predictions with experiments

Using the experimental setup described in Section 2 several flow boiling curves for a given absolute pressure and a given bulk velocity were measured. The thereby considered individual pressure–velocity combinations are summarized in Table 1. In all considered cases the temperature of the bulk liquid was kept constant at $T_{\text{b}} = 95\ ^{\circ}\text{C}$, which implies a subcooling of $\Delta T_{\text{sub}} = 16\ ^{\circ}\text{C}$ in the case $p = 1.5$ bar and $\Delta T_{\text{sub}} = 25\ ^{\circ}\text{C}$ in the case $p = 2.0$ bar, respectively. The heater wall temperature was varied within the interval $95^{\circ} \leqslant T_{\text{w}} \leqslant 150\ ^{\circ}\text{C}$. The slowest velocity in the lower pressure case ($p = 1.5$ bar) was chosen deliberately small, i.e., $u_{\text{b}} = 0.05$ m/s, to come as closest to the pool boiling limit as it was possible in

Table 1
Pressures and velocities of the bulk liquid considered in the boiling flow experiments

Absolute pressure p [bar]	Velocity of the bulk liquid u_{b} [m/s]		
1.5	0.05	0.39	1.17
2.0	0.20	0.39	1.17

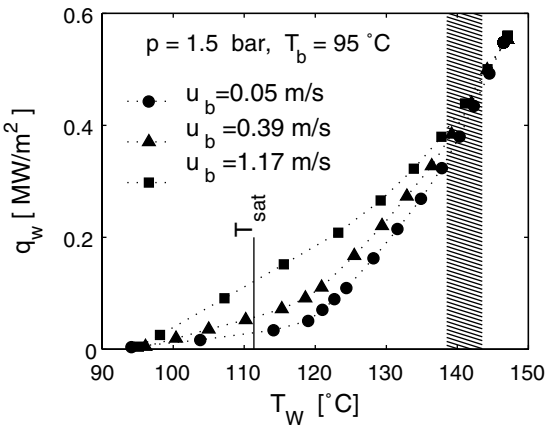

Fig. 11. Experimentally measured flow boiling curves at $p = 1.5$ bar absolute operating pressure and three different velocities of the bulk flow, $u_{\text{b}} = 0.05$, $u_{\text{b}} = 0.39$, $u_{\text{b}} = 1.17$ m/s, respectively.

the present experimental facility. As already noted in the former section the individual wall friction velocities u_τ associated with each bulk velocity u_b and required as model input were obtained using LDA measurements of the axial velocity profiles at the entrance of the heated test section. Fig. 11 shows all the boiling curves measured at $p = 1.5$ bar plotted into one single graph to illustrate the individual flow boiling regimes as already discussed schematically in Fig. 2. The approximately linear sections to the left of the curves indicate pure single-phase convection. Above the saturation temperature T_s the curves start to deviate from the single-phase linearity which marks the onset of the partially developed boiling regime (PDB). The notably different paths of the individual boiling curves demonstrate the strong influence of the flow rate in this temperature range. Looking at the wall temperatures, above which a non-linear increase of the heat flux can be observed, makes evident that the nucleate boiling sets in at about $\Delta T_s = 3$ °C wall superheat in the slow velocity case, $u_b = 0.05$ m/s, while the onset of boiling is located at about $\Delta T_s = 15$ °C in the high velocity case, $u_b = 1.17$ m/s. With increasing wall superheat the individual curves converge in the region around $T_w = 140$ °C (pattern-shaded interval), which indicates the transition to the fully developed boiling regime. There, the effect of the bulk flow rate is obviously insignificant and the total heat flux is dominated by velocity independent nucleate boiling mechanisms. As a consequence, irrespectively of the macrosopic flow velocity all boiling curves practically merge into one single branch.

Figs. 12 and 13 show the comparison between the total wall heat fluxes predicted by the BDL model with the corresponding experimental data at the two considered levels of the operating pressure, respectively. In all diagrams the saturation temperature T_s is marked by a thin vertical line. In addition to the results of the present BDL approach the heat fluxes predicted by other widely used models, due to Chen [16], Shah [12] and Kandlikar [11] are depicted as well.

The overall agreement between the predictions of the BDL model and the experimental data is good. Particularly in the high velocity case, $u_b = 1.17$ m/s, the BDL model predicts the shift of the onset of nucleate boiling to higher wall superheats accompanied by a relative reduction of the boiling component in the total heat flux very accurately. This indicates that the BDL model is capable to capture the strong flow induced suppression of the nucleate boiling in the PDB regime very well. For higher wall superheats, however, approaching the FDB regime, the agreement becomes worse especially in case of the lowest velocity considered ($u_b = 0.05$ m/s). This discrepancy can be explained by the fact that the present BDL model basically relies on the dynamics of a single bubble subject to a surrounding subcooled liquid flow field, which is assumed to remain unaffected by the presence of the vapour phase. Hence, it is conceivable that the predictions of the model are less accurate once phenomena related to the very complex multi-bubble dynamics become important. Due to the high bubble number densities, which are typically found on the heater surface in the FDB regime, a strong bubble–bubble interaction as well as a notable two-way coupling between the motion of the bubbles and the liquid phase occur. In such a regime bubbles tend to coalesce forming larger structures on the surface. Moreover, the motion of the bubbles pronouncedly affects the surrounding flow field of the liquid phase and vice versa. Considering these highly complex multi-phase flow phenomena there is certainly scope for further development of the present model in order to improve its accuracy particularly in the FDB regime.

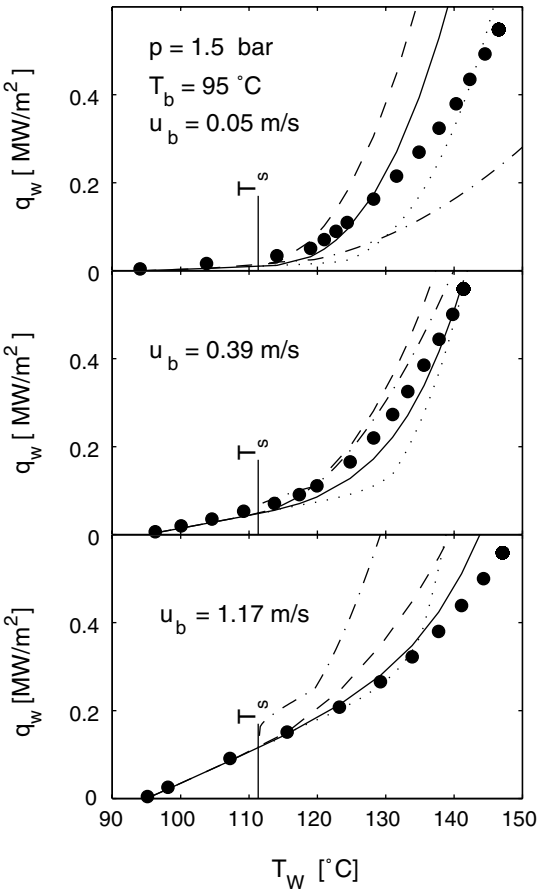

Fig. 12. Predicted flow boiling curves at $p = 1.5$ bar and three different velocities of the bulk flow, respectively: full line, '—', BDL; dashed line, '– – –', Chen; dashed dotted line '–·–·–' Shah; dotted line '· · ·' Kandlikar; symbols, '●', measurements.

The comparison with the results which were obtained with the models proposed by other authors and are also plotted in Figs. 12 and 13 reveals that

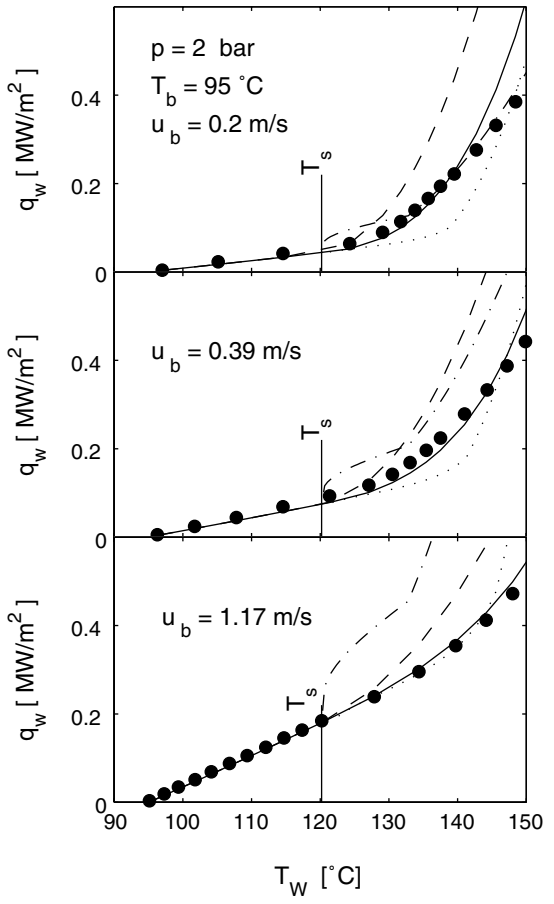

Fig. 13. Predicted flow boiling curves at $p = 2.0$ bar and three different velocities of the bulk flow, respectively: full line, '—', BDL; dashed line, '– – –', Chen; dashed dotted line '–·–·–' Shah; dotted line '···' Kandlikar; symbols, '●', measurements.

Chen's approach generally overpredicts the heat fluxes. This tendency towards overpredictions, which is also observed with many other Chen-type additive superposition correlations, can be explained by two main reasons. First, the empirical function for the suppression factor given in Eq. (11) used in Chen's model is obviously calibrated for saturated boiling, where the nucleate boiling heat transfer is typically higher than in subcooled boiling. Second, since the factor S_{Chen} depends on the bulk flow Reynolds number only, it practically represents a pure bulk flow quantity. It is therefore insensitive to local quantities like the wall superheat or wall shear stress, which can be expected to have a significant effect on a local phenomenon like the nucleate boiling heat transfer in a wall shear layer. As it was already pointed out in the former section, it was essentially these two shortcomings which motivated the authors to develop Chen's ansatz further to the present BDL proposal. The comparison with the corresponding results of the BDL model demonstrates that the predictive capability of Chen's superposition ansatz could be considerably improved by introducing an alternative model for the suppression of the nucleate boiling component as proposed in the BDL concept.

The results obtained using Shah's model [12] show a very good agreement in the FDB region in the case, at $p = 2.0$ bar and $u_{\mathrm{b}} = 0.2$ m/s. In the PDB regime the agreement is generally rather poor especially for the higher velocities, where considerable overpredictions are observed. The kink in the boiling curves marks the transition from the PDB to the FDB regime which is in Shah's model located at the superheat $\Delta T_{\mathrm{s}} = 0.5 \cdot \Delta T_{\mathrm{sub}}$. At this in principle arbitrarily determined point of transition the formulation switches from the correlation suggested for the PDB to the correlation suggested for the FDB regime which typically leads to an abrupt turn in the boiling curve. The approach due to Kandlikar [11] also prescribes a change in the formulation at the point of the transition from the PDB to the FDB regime. The location of this transition is determined in terms of the heat flux at the intersection between the extension of the single-phase line and the FDB curve multiplied by the factor 1.4. As shown in the results Kandlikar's proposal for locating the point of transition leads to accurate predictions in the PDB regime in the high velocity case. At the lower velocities the region which is dominated by single-phase convection extends too far into the nucleate boiling region, as the considerable underpredictions in the PDB region make evident.

In order to evaluate the performance of the BDL model in the case of stronger subcooling its predictions were also compared against experimental data obtained by Bibeau and Salcudean [13]. They carried out their

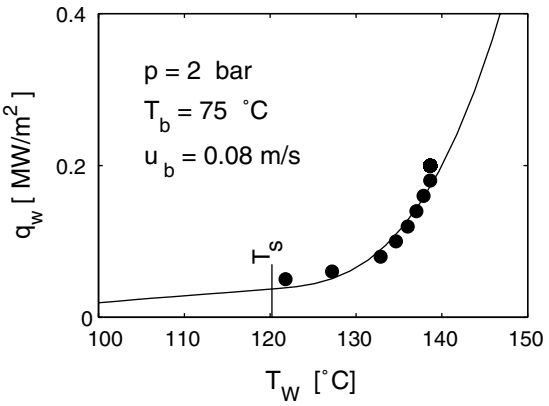

Fig. 14. Comparison at stronger subcooling; full line, '—', BDL; symbols, '●', measurements by Bibeau and Salcudean [13].

flow boiling measurements using an annular test section with the inner surface heated. The pressure was $p = 2$ bar and the bulk velocity was $u_b = 0.08$ m/s. The temperature of the bulk flow was $T_b = 75$ °C, which implies a subcooling of $\Delta T_{sub} = 45$ °C. As it is shown in Fig. 14, the predictions produced by the BDL model agree very well with the experiments. Due to the low flow rate the flow-induced suppression is considerably small, and, hence, the corresponding suppression factor S_{flow} does not deviate much from unity. Thus, the total suppression S is mainly due to effect of the subcooling. It turns out that the in the present case very dominant effect of subcooling is estimated very well in terms of the corresponding model parameter S_{sub} as given by Eq. (22).

5. Conclusion

In the present study a Chen-type superposition model is proposed to compute the effective wall heat flux in subcooled boiling flow. The proposed BDL model modifies the nucleate boiling contribution by introducing two suppression factors accounting for the effect of the flow forces and of the subcooling of the thermal boundary layer. The comparison with experimental data using water as working fluid shows good agreement especially in the partially developed boiling (PDB) regime. This good agreement in the PDB region, where the bulk flow rate exerts a significant effect on the nucleate boiling, indicates that the model captures the flow-induced suppression very well. Notable deviations occur primarily in the vicinity of the fully developed boiling (FDB) regime. These discrepancies clearly demonstrate the limits of the present model and give the scope for a further development. Thereby, the focus will have to be put on the consideration of the bubble–bubble as well as the bubble–liquid interactions, which are of great importance in the FDB regime.

Acknowledgements

The authors gratefully acknowledge the financial support from the Forschungsförderungsfond der gewerblichen Wirtschaft Österreich, the AVL List GmbH/Graz, the BMW Motoren GmbH/Steyr, and theKplus Virtual Vehicle Competence Centre/Graz.

References

[1] R. Mei, W. Chen, J.F. Klausner, Vapour bubble growth in heterogeneous boiling. I. Formulation, Int. J. Heat Mass Transfer 38 (1995) 909–919.
[2] R. Mei, W. Chen, J.F. Klausner, Vapour bubble growth in heterogeneous boiling. II. Growth rate and thermal fields, Int. J. Heat Mass Transfer 38 (1995) 921–934.
[3] W. Chen, R. Mei, J.F. Klausner, Vapour bubble growth in highly subcooled heterogeneous boiling, in: J.C. Chen (Ed.), Convective Flow Boiling, Taylor & Francis, Washington, DC, 1996, pp. 91–98.
[4] W.M. Rohsenow, Heat transfer with evaporation, in: Heat Transfer—A Symposium held at the University of Michigan During the Summer of 1952, University of Michigan Press, 1953, pp. 101–150.
[5] R.W. Bowring, Physical model based on bubble detachment and calculation of steam voidage in the subcooled region of a heated channel, OECD Halden Reactor Project Report HPR-10, 1962.
[6] A.E. Bergles, W.M. Rohsenow, The determination of forced convective surface boiling and heat transfer, Paper 63-HT-22 presented at the 6th National Heat Transfer Conference of the ASME-AIChE, Boston, 11–14 August 1963.
[7] J.L. Mostinskii, Calculation of heat transfer and critical heat fluxes in liquids, Teploenergetika 10 (1963) 66.
[8] M.G. Cooper, Saturation and nucleate pool boiling—A simple correlation, Inst. Chem. Eng. Symp. Ser. 86 (1984) 785.
[9] W. Leiner, D. Gorenflo, Methods of predicting the boiling curve and a new equation based on the thermodynamic similarity, in: V.K. Dhir, A.E. Bergles (Eds.), Pool and External Flow Boiling, ASME, New York, 1992, pp. 99–103.
[10] W. Leiner, Heat Transfer and convective pool boiling—General correlations based on the thermodynamic similarity, Int. J. Heat Mass Transfer 91 (1994) 763–769.
[11] S.G. Kandlikar, Heat transfer characteristics in partial boiling, fully developed boiling, and significant void flow regions of subcooled flow boiling, Trans. ASME J. Heat Transfer 120 (1998) 395–401.
[12] M. Shah, A general correlation for heat transfer during subcooled boiling in pipes and annuli, ASHRAE Trans. 83 (Part 1) (1977) 205–217.
[13] E.L. Bibeau, M. Salcudean, A study of bubble ebullition in forced-convective subcooled nucleate boiling at low pressure, Int. J. Heat Mass Transfer 37 (1994) 2245–2259.
[16] J.C. Chen, A correlation for boiling heat transfer to saturated fluids in convective flow, ASME preprint 63 HT34 presented at the 6th National Heat Transfer Conference, Boston, 1963.
[17] D. Butterworth, The correlation of cross flow pressure drop data by means of a permeability concept, UKAEA Report AERE-R9435, 1979.
[18] H.K. Forster, N. Zuber, Dynamics of vapor bubbles and boiling heat transfer, AIChE J. 1 (1955) 531–535.
[19] L.Z. Zeng, J.F. Klausner, D.M. Bernhard, R. Mei, A unified model for the prediction of bubble detachment diameters in boiling systems—II. Flow boiling, Int. J. Heat Mass Transfer 36 (1993) 2271–2279.
[20] N. Zuber, The dynamics of vapour bubbles in nonuniform temperature fields, Int. J. Heat Mass Transfer 2 (1961) 83–98.
[21] L.Z. Zeng, J.F. Klausner, R. Mei, A unified model for the prediction of bubble detachment diameters in boiling systems—I. Pool boiling, Int. J. Heat Mass Transfer 36 (1993) 2261–2270.

[22] R. Maurus, Bestimmung des Blasenverhaltens beim unterkühlten Strömungssieden mit der digitalen Bildfolgenanalyse, Doct. thesis, TU Munich, 2003.

[23] J.R. Wiebe, R.L. Judd, Superheat layer thickness measurements in saturated and subcooled nucleate boiling, Trans. ASME J. Heat Transfer 93 (1971) 455–461.